ACS OMEGA

Open Access

http://pubs.acs.org/journal/acsodf

Article

Effect of Polycaprolactone, Zinc Oxide, and Poly(ethylene glycol) on the Properties of Polylactic Acid Composite Fibers Obtained by Melt Electrospinning

Ferit Erdem, Halil Kandemir, and F. Burcu Alp*

Cite This: *ACS Omega* 2025, 10, 1457−1469

Read Online

ACCESS | Metrics & More | Article Recommendations | Supporting Information

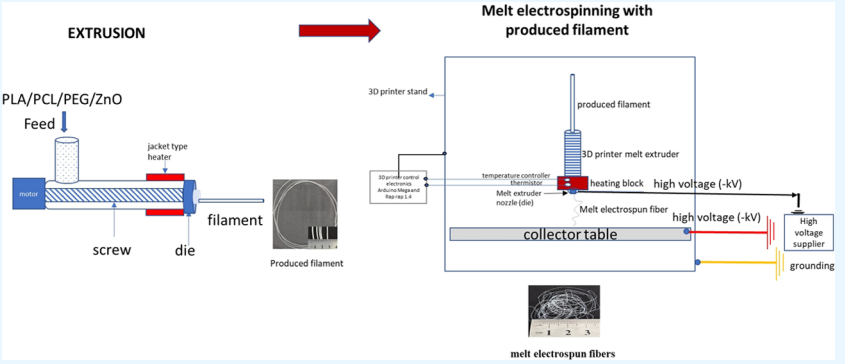

ABSTRACT: Polylactic acid (PLA) composite fibers were obtained using melt electrospinning, in which a high voltage was applied to the nozzle of the 3D printer. Filaments for melt electrospinning were prepared by using an extruder operated at 155 °C. PLA was mixed with polycaprolactone (PCL; 95:5, 90:10, and 85:15 by wt %), zinc oxide (ZnO; 0.1 phr), and poly(ethylene glycol) (PEG; 1 phr). The prepared filaments and fibers were characterized by Fourier-transform infrared spectroscopy (FTIR), contact angle measurements, thermal gravimetry (TGA), differential scanning calorimetry (DSC), and dynamic mechanical analysis (DMA). The measured contact angles of the filaments were in the range of 60.33° (±4.04) to 78° (±2.65), while the melt-electrospun fibers were in the range of 110.17° (±0.29) to 128.5° (±1.32). Melt electrospinning significantly increased the contact angle. According to the DSC analysis, the addition of 0.1% ZnO and 1% PEG increased the degree of crystallinity of PLA from 19.63 to 27.48% in the filaments and 11.54 to 20.79% in the fibers. The Avrami constant (n) values of the filaments and fibers were found in the range between 2.62−3.97 and 2.75−3.95, respectively. It was shown that the crystallization was controlled by nucleation. DMA analysis indicated that melt electrospinning and the addition of PCL decreased the storage modulus of the filaments, thereby increasing their plasticity.

1. INTRODUCTION

Recently, studies on the development of environment-friendly materials that can replace traditional plastic materials to prevent environmental pollution have increased. Biodegradable polymers are evaluated as a solution to the waste problem.[1] Due to its production from natural resources and biodegradability, studies are carried out to use polylactic acid (PLA) instead of some petroleum plastics. PLA has a higher modulus and strength than many petroleum-based aliphatic polyesters.[2,3] It has good optical, physical, mechanical, and barrier properties.[4] Carbon dioxide (CO_2), oxygen (O_2), nitrogen (N_2), and water vapor permeability coefficients of PLA are lower than those of polystyrene (PS) but higher than those of poly(ethylene terephthalate) (PET).[5,6] Semicrystalline PLA exhibits a glass transition temperature (T_g) and melting temperature (T_m) similar to those of many thermoplastic polymers. Above T_g, approximately 58 °C, PLA shows elastic properties, while below T_g it behaves as a brittle polymer.[7] The brittleness of PLA is a disadvantage in practical applications. In general, the most effective method for improving the toughness of a brittle polymer is to blend it with soft, ductile polymers.[8,9] Polycaprolactone (PCL) is a soft, biocompatible, and biodegradable semicrystalline polyester.[10−12] The T_g of PCL is around −60 °C and its melting temperature is in the range of 55−70 °C. PCL degrades at a slower rate than polyglycolide, poly(D,L-lactide), or copolymers.[13] PLA and PCL blends are suitable for use in a variety of applications such as packaging,

Received: October 8, 2024
Revised: December 25, 2024
Accepted: December 26, 2024
Published: January 3, 2025

cardiovascular, wound dressings, and tissue engineering.[14−17] Melt blending of PCL with brittle PLA has been reported to provide flexibility in the polymer blend and improve barrier properties.[18]

The effect of various nanoparticles (NPs) in PLA/PCL blends on their microstructure has been widely investigated.[11,19,20] Some NPs used with PLA include layered silicates, organoclays, carbon nanotubes, hydroxyapatite (HA), layered titanate, and aluminum hydroxide.[2] Among potential NPs, ZnO is preferred due to its excellent antibacterial, UV protective, and photocatalytic properties.[21−24] ZnO NPs may play a fundamental role in the degradation, crystallization, UV absorption, and mechanical properties of polymers.[25−27] It has been reported that ZnO improves the barrier properties of polymer composites,[28−32] while its mechanical properties generally reduce the elongation at break[28,31−34] and increase the tensile strength/yield stress.[28,35]

The thermal stability of PLA is related to the amount and volatility of the plasticizer used.[36] As a hydrophilic polymer, poly(ethylene glycol) (PEG) is an effective plasticizer for PLA, which modifies the toughness, hydrophobicity, cell affinity, and degradation rate;[37−39] therefore, it is also used as a crystallization additive.

Many studies have been performed on the electrospinning method for preparing nanostructured materials or for functionalizing the material surface with functional electrospun nanofibers.[40] Electrospinning is a technique that produces nonwoven fibers by depositing a single jet of electrical charge onto a negatively charged, grounded collector. Electrospun materials can be produced with desired structural properties using the parameters and solution properties used in the electrospinning process. In addition, a higher surface-to-volume ratio can be adjusted structurally.[41−43] It has been reported that more than 100 different types of organic polymers directly produce nanofibers by the solution electrospinning method.[44] Most studies have used zein[45,46] or a combination of zein−polyhydroxyalkanoate (PHA).[47] Similarly, cellulose,[48] chitosan,[30] PLA,[49] poly(vinyl alcohol) (PVA),[50] and PCL[51] have been widely used in the production of many biobased electrospun materials. However, there are many problems associated with the use of solvents in the solution electrospinning method. It has been reported that some conductive polymers are not suitable for solution electrospinning because of their poor solubility in common solvents, and their high solution conductivity makes it difficult to create a stable jet. In addition, it is difficult to dissolve polyethylene and polypropylene in suitable solvents for electrospinning.[44] Besides, the solvents used in the solution electrospinning method are very expensive, and toxic waste must be recovered; however, the recovery of the solvent in an electrospinning process is difficult. Since no solvent is used in the melt electrospinning method, there is no need to consider solvent recovery and toxicity of the solvent.[52] Rivera and Hudson[53] produced PLA electrospun using the melt electrospinning method on a 3D printer. They tried to highlight melt electrospinning, as well as rigid plastic 3D printing using a single FFF (fused filament fabrication) extruder. They performed a series of tests by changing the extrusion speed, nozzle temperature, and fill % print density to determine the melt-electrospinning process parameters. The optimum process parameters were determined to be an extrusion speed of 10 mm min^{-1}, nozzle temperature of 290 °C, and fill % print density of 10%. They showed that by combining the flexibility of the produced electrospun fibers with the structure of hard plastic, objects, and sensors that provide actuation, sensing, and tactile experiences can be produced. Shahverdi et al.[54] used the melt electrowriting (MEW) process to fabricate PLA, PCL, and PLA/PCL scaffolds. MEW combines the two well-established techniques of fused deposition modeling (FDM) and electrospinning. They used a commercial FDM 3D printer with modifications for electrospinning. PCL and PLA filaments were purchased. The fabricated scaffolds were characterized and compared in terms of their fiber morphology, pore structure, mechanical properties, and interactions with water. The MEW process parameters used in this study were a feed rate of 10 μL min^{-1}, collector temperature of 60 °C, printing speed of 65 mm s^{-1}, and a distance of 5 mm between the nozzle head and collector. The extruder temperature of the 3D printer was 230 °C for PLA and 100 °C for PCL, and the applied high voltage was 4.5−5 kV for PCL and 6−6.5 kV for PLA. It has been reported that fibers had a uniform cylindrical shape with a nearly constant diameter (for PCL: from 5 to 15 μm; for PLA: from 15 to 25 μm) and a measured contact angle of 90 ± 10° for PLA and 100 ± 5° for PCL. Li et al.[55] prepared oil/water separation PLA membranes by melt electrospinning of PLA powder. Experiments were conducted at a temperature of 25 ± 5 °C and humidity of 50 ± 5% using a self-assembled melt electrospinning apparatus consisting of a high-voltage electrostatic generator, a temperature-controlled heater, a barrel, a customized umbrella-like spray head, and a flat collecting plate. According to the orthogonal experimental design results, they reported that the optimal conditions for melt electrospinning were a temperature of 220 °C, a collector distance of 8 cm, and a voltage of 45 kV. The diameter and the contact angle of the melt-electrospun PLA fiber were found to be 6.47 μm and 122°, respectively. Curcumin-loaded PCL fibers were prepared by both melt and solution electrospinning methods.[56] Melt electrospinning was carried out at 180 °C. The distance from the tip to the collector was 15 cm, +20 kV was applied to the melt, and −10 kV was applied to the flat collector. In solution electrospinning, the injection rate was 0.5 mL h^{-1}, the distance from the tip to the collector was 10 cm, and +10 kV voltage was applied to the needle tip. The samples obtained by both methods were characterized by scanning electron microscopy (SEM), fluorescence microscopy, differential scanning calorimetry (DSC), X-ray diffraction (XRD), and atomic force microscopy (AFM). The diameters of the melt and solution electrospun fibers were found to be 4.25 ± 1.17 and 4.27 ± 1.49 μm, respectively. The morphology of the electrospun fibers was found to be significantly dependent on the production method. It was reported that melt-electrospun fibers exhibited a smooth surface and high crystallinity, while solution electrospun fibers exhibited more amorphous regions and a porous structure. Melt-electrospun fibers have been found to be more suitable for drug delivery applications than solution electrospun fibers, as they can slowly release drugs owing to their high crystallinity. Polyether-*block*-amide (PEBA) fibers were prepared using both melt and solution electrospinning methods.[57] The effects of the process parameters of both methods on fiber diameters and morphology were investigated. PEBA pellets were produced in a 1.5 mm-diameter filament form for melt electrospinning using a filament extruder that included grinding, melting, extrusion, cooling in a cold water bath, and stretching in a roll system. The PEBA filament was fed at a

https://doi.org/10.1021/acsomega.4c09181
ACS Omega 2025, 10, 1457−1469

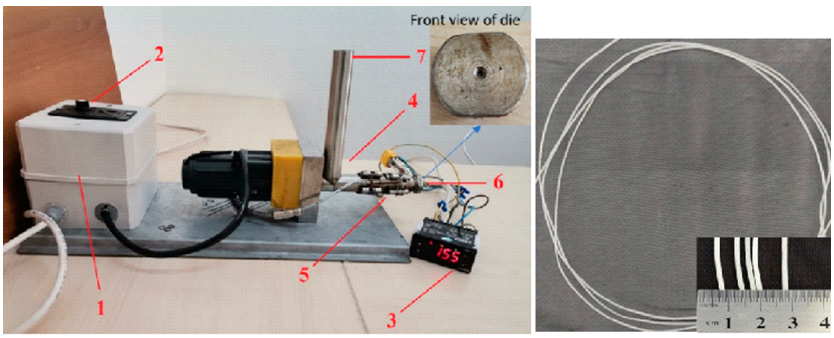

Figure 1. (a) Single-screw mini-extruder: 1− power supply, 2 − motor switch, 3 − temperature controller, 4 − extruder, 5 − jacket-type heater, 6 − die, and 7 − polymer feed. (b) Sample of filament obtained by a mini-extruder.

flow rate of 5 mm min^{-1} to the extruder with a 0.4 mm-diameter nozzle. A homogeneous solution was prepared by dissolving the PEBA pellets in either glacial acetic acid or butanol at 60 °C with magnetic stirring at 250 rpm for 5 h. A full factorial experimental design was performed by varying the process parameters for both methods. The electrospun samples were characterized using SEM, thermal gravimetric analysis (TGA), Fourier-transform infrared spectroscopy (FTIR), XRD, and optical tensiometry. The minimum average fiber diameter of the melt and solution electrospun fibers was found to be 1.92 ± 3.31 and 0.37 ± 0.34 μm, respectively. It was reported that electrospinning of PEBA did not change its thermal and chemical properties while decreasing the fiber diameter increased its hydrophobicity. Although larger fibers were produced using melt electrospinning, it was found that not using a solvent in the process was advantageous. Therefore, it has been reported that it is more suitable for higher-efficiency production, especially in cases in which super-micrometer fibers are required.

Studies have shown that melt electrospinning increases the crystallinity, hydrophobicity, and mechanical properties of polymers. In this study, melt electrospinning was used for preparing the PLA/PCL/ZnO/PEG composite fibers. Melt electrospinning equipment was built by other inspiring works in the literature.[53] The filaments used in melt electrospinning were produced using an extruder. The preparation of the composite PLA/PCL/ZnO/PEG fibers using melt electrospinning is a novelty of this study. PLA was mixed with PCL to improve its brittleness. ZnO nanoparticles were selected to improve the crystalline and mechanical properties of the polymer mixture. PEG was used as a crystallization modifier to ensure the distribution of the ZnO NPs in the polymer matrix. The prepared filaments and fibers were characterized using FTIR spectroscopy, contact angle measurements, TGA, DSC, and dynamic mechanical analysis (DMA) to examine the effects of organic additives (PCL and PEG), inorganic additives (ZnO), and melt electrospinning on PLA properties.

2. EXPERIMENTAL SECTION

2.1. Materials. PLA (Indigo biopolymer 2003D, Natureworks), PCL (Sigma-Aldrich; MW: 80,000), PEG 400 (LabShop41), and ZnO (Ege Nanotek, dp: 40 nm) were used to prepare the filaments.

2.2. Hansen Solubility Parameters. The compatibility of the surfaces of the polymers used (PLA/PCL), the organic additive used as a crystallization regulator (PEG 400), and the inorganic additive (ZnO NP) used to improve the barrier properties was checked using solubility parameter criteria.[58] The Hansen solubility parameters of the polymers were calculated using the group contribution method as in the previous study,[13] and the partial solubility parameters of ZnO were taken from Hansen.[58]

2.3. Preparation of Filaments by Extrusion. Filaments were prepared using a handmade mini-extruder with a length of 14 cm, a diameter of 2.4 cm, a nozzle head diameter of 2 mm, and a rotation speed of 50 rpm at 155 °C, as shown in Figure 1a. A temperature-controlled jacket-type heater was used for heating. The PLA and PCL mixture was prepared by dry mixing in the ratios of 95:5, 90:10, and 85:15, by weight %. ZnO was dispersed in PEG by vortexing and then added to the PLA/PCL mixtures. Extruded filament samples were obtained in the diameter range of approximately 1.5−2.0 mm, as shown in Figure 1b. The prepared filaments and their contents are presented in Table 1.

Table 1. Sample Codes and Compositions of the Prepared Filaments

sample no.	sample code	PLA (wt %)	PCL (wt %)	ZnO (phr)	PEG (phr)
1	PLA	100			
2	PLA- ZnO-PEG	100		0.1	1
3	PLA95-PCL5	95	5		
4	PLA95-PCL5-ZnO-PEG	95	5	0.1	1
5	PLA90-PCL10	90	10		
6	PLA90-PCL10-ZnO-PEG	90	10	0.1	1
7	PLA85-PCL15	85	15		
8	PLA85-PCL15-ZnO-PEG	85	15	0.1	1

2.4. Melt Electrospinning. Melt electrospinning was performed using a handmade 3D printer, as shown in Figure 2. The printer's extruder is an FFF model with a nozzle diameter of 0.4 mm and was heated up to 300 °C. A high voltage was applied using a high-voltage supplier.

The printer was designed to be controlled by both the computer and LCD screen. The *X*, *Y*, and *Z* axes are provided with motion-drive motors. Arduino MEGA 2560 and RepRap Ramps version 1.4 control cards were used for 3D automation. The desired distance (distance from the nozzle to the collector) and extrusion temperature were set, and the printer extruder was heated. Then, the filament pusher (in Figure 2, number 4), which provides the movement of the filament in

https://doi.org/10.1021/acsomega.4c09181
ACS Omega 2025, 10, 1457−1469

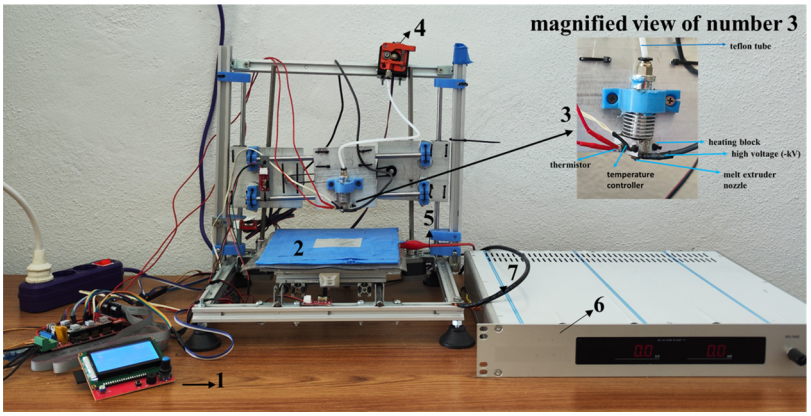

Figure 2. 3D printer: 1 − LCD screen, 2 − collector table, 3 − melt extruder, 4 − filament pusher, 5 − high voltage (+kV), 6 − high-voltage supplier, and 7 − ground line.

the Teflon tube, was set at the desired extrusion speed and operated. The electrospinning process was performed by applying a high voltage to the melt coming from the nozzle tip (magnified view of number 3 in Figure 2). A high voltage was applied to the nozzle tip at −kV and to the collector table at +kV with a high-voltage supplier (Figure 2, number 5). The obtained melt-electrospun fibers are shown in Figure 3.

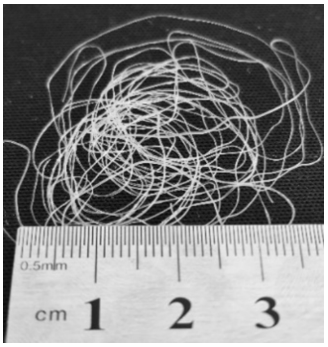

Figure 3. Sample of melt-electrospun fibers.

The melt electrospinning parameters such as the distance from the nozzle to the collector (15/30/45 mm), voltage (5/10/15 kV), extrusion temperature (230/240/250 °C), and extrusion speed (5/10/15 mm min^{-1}) were changed to obtain the minimum fiber diameter using a neat PLA filament. The diameters of the fibers were determined using optical microscopy (Olympus BX51) and SEM (Fei Quanta Feg 250). The PLA/PCL/PEG/ZnO composite filaments were melt-electrospun under the obtained minimum fiber diameter conditions.

2.5. Structural Characterization of the Prepared Filaments and Fibers. The functional groups of the samples were determined via FTIR spectroscopy using an ATR kit (Jasco FTIR-4700 Spectrometer). Measurements were performed in the range of 400−4000 cm^{-1}. For samples containing ZnO, measurements were performed in the range of 350−4000 cm^{-1}.

The ZnO contents of the filaments and fibers prepared using inorganic additives were investigated using SEM (Fei Quanta Feg 250). Energy-dispersive X-ray spectroscopy (EDX) analyses of the filaments were performed on the cross-section, whereas the fibers were on the surface by selecting at least 2 different areas, and the average values were obtained.

Contact angle measurements of the samples were performed using a goniometer (Rame-Hart 100-00-230 model). The measurements were made at 3 different points, and the average was recorded. Images of the measurements were obtained by taking photographs through the lenses. Wide angles were determined by subtracting the measured angle from 180°.

2.6. Thermal Characterization of the Prepared Filaments and Fibers. The thermal stabilities of the filaments and fibers were investigated by TGA (Shimadzu TGA-51). For the TGA analysis, 10 mg samples were loaded into an alumina pan and heated at a rate of 10 °C min^{-1} under a N_2 atmosphere (40 mL min^{-1}) from room temperature to 600 °C.

The melting points and the degree of crystallinity (X_c) of the samples were determined by DSC (Shimadzu DSC-60). For the DSC analysis, samples (3 mg) were placed in a covered aluminum pan under a nitrogen atmosphere (40 mL min^{-1}) and heated at a rate of 10 °C min^{-1} from room temperature to 600 °C. The degree of crystallinity of the samples from the DSC melting peaks was determined using eq 1

$$X_c = \frac{\Delta H_m}{w\Delta H_f^0} \times 100 \quad (1)$$

where ΔH_m is the melting enthalpy of the samples (J g^{-1}), ΔH_f^0 is the heat of fusion of PLA (93.6 J g^{-1})[59] at 100% crystallinity, and w is the weight fraction of PLA in the samples.

The crystallization behavior of the samples was also investigated based on the nonisothermal crystallization peak area using the Avrami model. The Avrami model is given in eq 2[60]

$$X_t = 1 - \exp(-kt^n) \quad (2)$$

where X_t, n, t, and k are the relative crystallinity, Avrami constant, crystallization time, and crystallization rate constant, which include both nucleation and growth rate parameters, respectively. The Avrami model can be linearized as in eq 3

$$\ln(-\ln(1 - X_t)) = \ln k + n \ln t \quad (3)$$

where n and $\ln k$ are obtained from the slope and intersection of the Avrami plot, respectively. Relative crystallinity (X_t) can be defined as a function of time using eq 4

https://doi.org/10.1021/acsomega.4c09181
ACS Omega 2025, 10, 1457−1469

$$X_t = \frac{\int_0^t \left(\frac{dH}{dt}\right) dt}{\int_0^\infty \left(\frac{dH}{dt}\right) dt} \quad (4)$$

where H is the crystallization enthalpy during the infinitesimal time interval dt, and ∞ is the time at the end of crystallization.

Dynamic mechanical analysis (DMA) was performed using a PerkinElmer DMA 8000 instrument. Analyses were carried out using the single cantilever bending method at a heating rate of 5 °C min^{-1} from room temperature to 240 °C in an N_2 environment with a frequency of 1 Hz.

3. RESULTS AND DISCUSSION

3.1. Thermodynamic Compatibility Analysis with Hansen Solubility Parameter. The calculated solubility parameters are listed in Table S1. The R_a and RED values calculated from partial solubility parameters are provided in Table S2. Since the RED number values found were less than 1, it indicates that the materials used in the filament preparation are thermodynamically compatible.[58]

3.2. Minimum Fiber Diameter Optimization in Melt Electrospinning. PLA was melt-electrospun at different temperatures, voltages, speeds (extrusion speed), and heights (distance from the tip to the collector). The diameters of the obtained fibers determined by optical microscopy and SEM are listed in Table S3. The minimum fiber diameter was 37.80 μm obtained at 230 °C, 15 mm height, 10 kV voltage, and 0.167 mm s^{-1} extrusion speed. These conditions were considered optimum, and the composite PLA filaments were melt-electrospun under optimum conditions. It was observed that distances > 30 cm have less effect on the instability of the fibers and the electrical field on the molten jet and distances between 15 and 25 cm are considered appropriate, and it is possible to adjust and reduce the diameter (higher stretching and orientation of the fibers) by increasing the distance.[61]

The fiber diameters of melt-electrospun composite fiber measurement photographs taken using the optical microscope lens and the measured fiber diameters are provided in Tables S8 and S9, respectively. The changes in the fiber diameters of the melt-electrospun composite fibers under optimum conditions are shown in Figure 4. The average fiber diameters were observed in the range of 37.83 ± 1.89 to 341.66 ± 2.89 μm. It is thought that the wide range of fiber diameters is due to the process parameters and flow properties of the polymer mixture melt obtained in the presence of additives. Similarly, it has been reported that the increased interfacial tension between the phases of PLA/PCL blend fibers exhibits a higher average electrospun fiber diameter compared to PLA fibers. Since the amount of polymer was quite low in the solution electrospinning method, the diameters of the fibers obtained were much lower than those obtained by melt electrospinning. Yu et al.[62] observed that melt electrospinning leads to higher fiber diameters and higher volume scaffolds (3D textures) than solution electrospinning. It was observed that the fiber diameter increased with the addition of ZnO and PEG. Nazari and Garmabi[63] stated that in the melt-electrospinning process of PLA/PEG mixtures, the fibers become thinner as the temperature, applied voltage, and PEG content increased, and the most effective factor on the fiber diameter was the PEG concentration. Increasing the PEG content to 20−30 wt %, a temperature of 220 °C, and a voltage of 40 kV reduced the fiber diameter. In this study, 1 phr PEG was added. With the addition of ZnO, the thinning of the fibers was prevented by affecting the flow properties (increasing the melt viscosity). According to the results, a decrease in the fiber diameter was observed with the addition of PCL, increasing from 5 to 15% by weight. It was observed that the fibers became thinner due to the plasticizing effect of PCL. Among the composite fibers, the lowest fiber diameter was observed for the PLA-ZnO-PEG composite fiber.

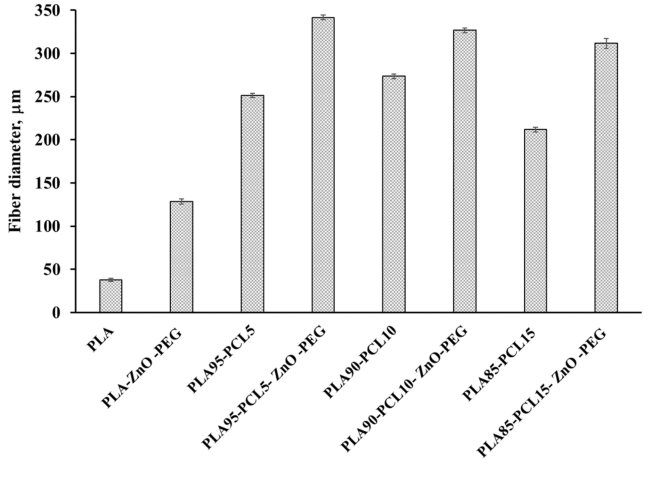

Figure 4. Diameters of the electrospun fibers.

3.3. Structural Characterization. The FTIR spectra for PLA, PCL, PEG, and ZnO used in filament preparation are shown in Figure 5, and those of the prepared filaments are shown in Figure 6. It was previously reported in the literature that characteristic infrared bands of PLA located at 1746 cm^{-1} were due to C═O stretching, at 2995 cm^{-1} was due to $-CH_3$ asymmetric stretching, at 2946 cm^{-1} was due to $-CH_3$ symmetric stretching, and at 1200 cm^{-1} was due to C−O stretching.[64] The bands at 3278 and 3221 cm^{-1} were due to the OH−COOH functional groups of lactic acid.[65] The bands at 1395−1440 cm^{-1} were due to the bending of C−O−H, at 1163−1210 cm^{-1} were due to the stretching of the C−O saturated ester, and at 2840−3000 cm^{-1} were due to the stretching of C−H.[66] The C═O stretching was observed at 1748 cm^{-1}, the $-CH_3$ asymmetric stretching was observed at 2996 cm^{-1}, the C−H stretching was observed at 2917 cm^{-1}, the bending of C−O−H was observed at 1453 and 1364 cm^{-1}, and the stretching of the C−O saturated ester was observed at 1185 and 1084 cm^{-1} in PLA. The characteristic infrared bands of PCL at 2949 and 2865 cm^{-1} were CH_2 stretching, at 1727 cm^{-1} were carbonyl stretching, at 1293 cm^{-1} were C−O and C−C stretching in the crystalline phase, at 1240 cm^{-1} was asymmetric COC stretching, at 1190 cm^{-1} was OC−O stretching, at 1170 cm^{-1} was symmetric COC stretching, and at 1157 cm^{-1} was C−O and C−C stretching in the amorphous phase. The band at 1292 cm^{-1} was due to the backbone C−C and C−O stretching modes in the crystalline PCL.[67] CH_2 stretching was observed at 2941 cm^{-1}, and strong bands, such as carbonyl stretching, were observed at 1719 cm^{-1}, and a symmetric COC stretching was observed at 1168 cm^{-1} in PCL.

The characteristic bands of PEG 400 at around 3400 cm^{-1} were ascribed to O−H stretching, at 2862 cm^{-1} was attributed to the C−H stretching vibrations of the $-CH_2$ group, at 1245 cm^{-1} was attributed to the C−O stretching vibration, at 1452 cm^{-1} was attributed to the C−H bending vibrations of the $-CH_2$ group, and at 937 cm^{-1} was assigned to the C−O−C

https://doi.org/10.1021/acsomega.4c09181
ACS Omega 2025, 10, 1457−1469

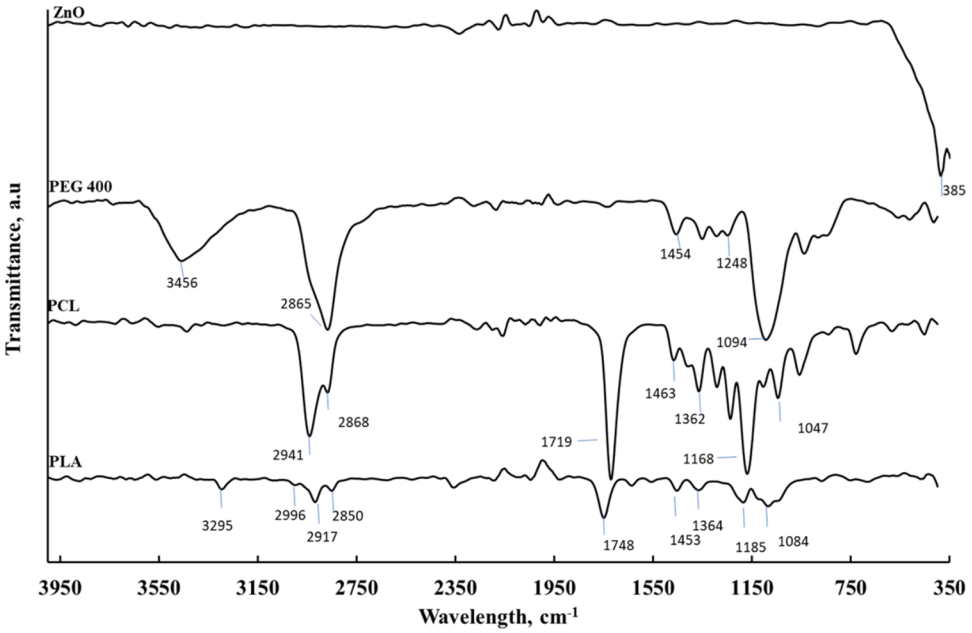

Figure 5. FTIR spectra of the raw materials.

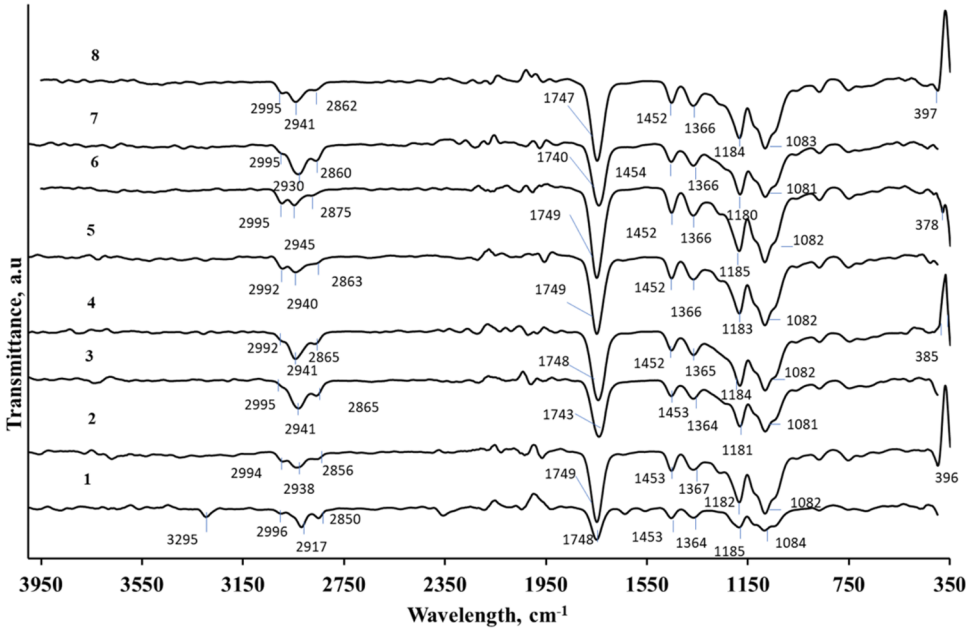

Figure 6. FTIR spectra of the prepared filaments.

symmetrical stretching.[68] O−H stretching was observed at 3456 cm^{-1}, C−H stretching vibrations of the $-CH_2$ group were observed at 2865 cm^{-1}, C−H bending vibrations of the $-CH_2$ group were observed at 1454 cm^{-1}, and C−O−C symmetrical stretching was observed at 1094 cm^{-1}.

The peak at 423 cm^{-1} belongs to the zinc−oxygen coordination in the FTIR spectrum of ZnO.[69] Zinc−oxygen coordination was observed at 385 cm^{-1} in the ZnO sample. In addition, a small broad peak at 3300−3500 cm^{-1} indicates the presence of OH groups or water molecules in the powder product.

In the FTIR spectra of the prepared filaments (Figure 6), the CH_3 asymmetric stretching peak of PLA at 2996 cm^{-1} was observed in the filaments in the range of 2992−2996 cm^{-1}, and the CO stretching peak of PLA at 1748 cm^{-1} was observed in the filaments in the range of 1740−1749 cm^{-1}. The C−H stretching vibration peak at 2862 cm^{-1} of PEG was observed at 2856 cm^{-1} in filament 2. Filament samples 3, 5, and 7 were of PLA−PCL mixtures. The peaks corresponding to both PLA and PCL were observed in these samples. The peaks corresponding to ZnO in samples 2, 4, 6, and 8 were observed at 396, 385, 378, and 397 cm^{-1}, respectively. The functional groups of the filaments indicate a combination of these components.

EDX analysis of ZnO-containing filaments at the cross-section and fibers on the surface was performed, as shown in Tables S4 and S5. The investigation of a full screen for ZnO detection showed that both filaments and fibers have zinc oxide in their structures. The limitation of EDX analysis in scanning electron microscopy is that data is collected from the

https://doi.org/10.1021/acsomega.4c09181
ACS Omega 2025, 10, 1457−1469

surface of the sample, which can sometimes be misleading. Thus, the good dispersion of ZnO particles in the whole polymer matrix could not be proven with this analysis. For sample 4, the ZnO contents of the filament and fiber were determined as 0.22 and 0.26%, respectively, which are greater than the initial amount. This may be due to the agglomeration of ZnO in the analysis area. Finally, it can be concluded that the ZnO nanoparticles are not dispersed evenly in the polymer matrix.

It is known that the contact angle is a common way to measure the wettability of a material surface.[70] The contact angle depends on the relative magnitude of the attractive forces between the molecules of the liquid and the attractive forces between the liquid and solid. If the attractive forces between the liquid molecules (cohesion forces) are greater than the attractive forces between the liquid and the solid (adhesion forces), the liquid drop attracts itself and takes a spherical shape instead of spreading on the surface. In this case, the contact angle becomes large, and there is little contact between the liquid and solid surface (hydrophobic property). Contact angle measurement photographs taken through the lens are presented in Tables S6 and S7. The measured contact angles of the filaments and fibers are provided in Table 2 and Figure 7.

Table 2. Measured Contact Angles of the Filaments and Fibers

	contact angle (deg)	
sample no.	filament	fiber
1	60.33 ± 4.04	114.00 ± 1.73
2	61.33 ± 1.53	113.00 ± 0.00
3	70.50 ± 4.77	111.00 ± 1.73
4	67.67 ± 0.58	117.67 ± 0.58
5	70.00 ± 5.20	125.50 ± 0.00
6	76.33 ± 3.79	128.50 ± 1.32
7	78.00 ± 2.65	121.00 ± 1.00
8	71.67 ± 2.52	110.17 ± 0.29

The contact angle of the neat PLA filament was 60.33°. The addition of ZnO and PEG to PLA (sample 2) had no effect on the contact angles, considering measurement errors. The contact angle increased with increasing PCL content. It was observed that the contact angles were in the range of 67−78° with the addition of PCL. The contact angles of the fibers obtained by melt electrospinning were in the range of 111−128°. This confirmed that melt electrospinning provides hydrophobic properties. Sharma and Satapathy[71] demonstrated the hydrophobic properties of electrospun fibers and stated that they induce the self-cleaning properties of the fibers; therefore, they are potential candidates for numerous biomedical applications, especially in drug delivery systems.

3.4. Thermal Characterization. Thermal characterization of the filaments and fibers was performed by TGA, DSC, and DMA. Figure 8 shows a thermogram of the prepared PLA composite filaments and fibers. The degradation start temperatures (T_{deg}) of the samples were determined from the thermograms and are listed in Table 3. All samples were thermally stable up to 240 °C. The T_{deg} values of the samples were in the range of 314−242 °C. Degradation of the neat PLA filament started at 294 °C. The addition of PCL to the PLA filament increased T_{deg}, while the addition of ZnO and PEG decreased it. The T_{deg} of the melt-electrospun neat PLA fiber was 285 °C. The addition of PCL resulted in the opposite behavior of increasing T_{deg} observed in the filaments. All additives reduced the T_{deg} of the spun PLA fibers.

The nonisothermal DSC heating profiles of the samples are shown in Figure 9. The T_g values for filament samples 1 and 2 (neat PLA and PLA_ZnO0.1_PEG1) were observed at 63.9 and 61.66 °C, respectively, which are close to those obtained from the DMA analysis of the loss modulus curve (Figure 11c,d). When PCL was added to PLA, the T_m of PCL was observed in DSC analyses because the T_m of PCL was close to the T_g of PLA (Samples 3−8). The T_g values obtained from DMA analysis are listed in Table 3. The addition of PCL slightly reduced the T_g of PLA, while melt electrospinning increased it. The T_m values of the filaments were between 148.9 and 155.51 °C and those of the fibers were between 149.81 and 156.66 °C. The T_m decreased with the addition of PCL or ZnO-PEG to PLA, whereas when PCL and ZnO-PEG were added together, the $T_m$increased. Melt electrospinning did not significantly affect the T_m. The crystallization temperatures (T_c) of the filaments were between 103.17 and 117.04 °C and those of the fibers were between 106.74 and

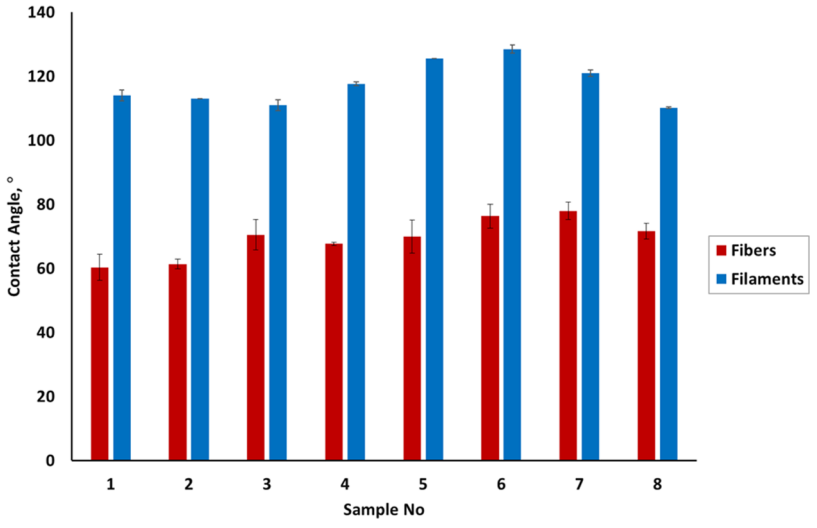

Figure 7. Plot of measured contact angles of the filaments and fibers.

https://doi.org/10.1021/acsomega.4c09181
ACS Omega 2025, 10, 1457−1469

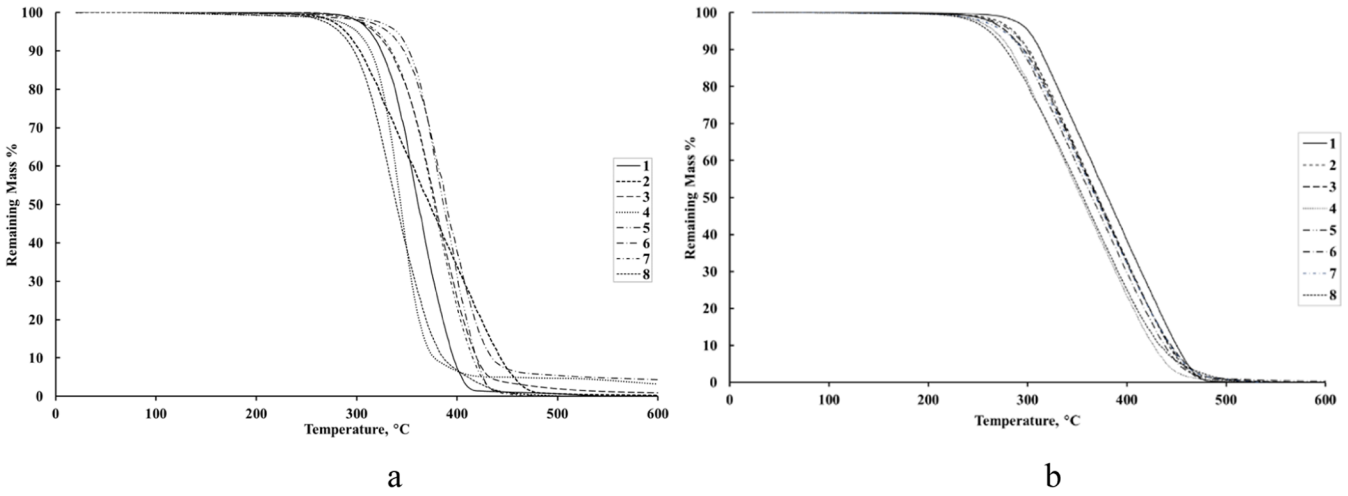

Figure 8. TGA thermograms of (a) filaments and (b) fibers.

Table 3. Comparison of T_g, T_m, T_c, and T_{deg} of the Filaments and Fibers

	T_g [°C]		T_m [°C]		T_c [°C]		T_{deg} [°C]	
sample no.	filament	fiber	filament	fiber	filament	fiber	filament	fiber
1	64.1	66.05	151.13	150.08	117.04	115.63	294	285
2	62.52	64.47	149.57	149.81	109.89	116.08	273	269
3	63.39	63.70	149.56	151.29	112.85	115.86	296	259
4	63.33	65.69	154.4	155.94	103.17	108.71	281	246
5	60.79	64.78	149.77	151.94	114.98	117.82	314	262
6	61.39	65.83	149.71	151.8	112.92	117.76	299	259
7	61.33	63.7	148.9	155.38	109.9	107.77	300	251
8	64.08	64.94	155.51	156.66	105.28	106.74	264	242

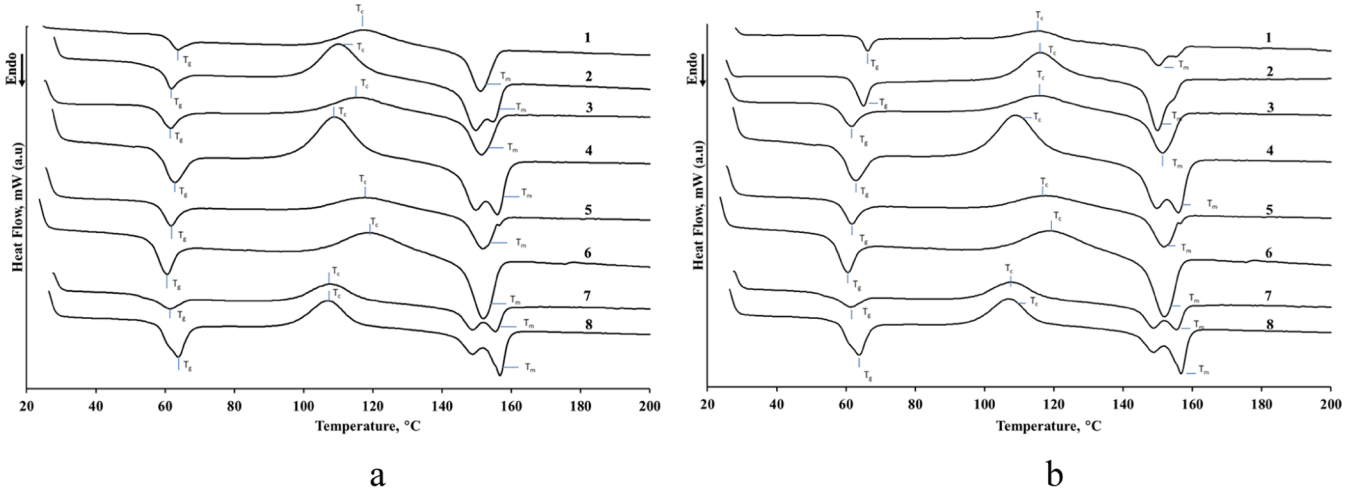

Figure 9. DSC curves of (a) filaments and (b) fibers.

117.82 °C. It was observed that all additives used in the PLA filament reduced the T_c. The X_c values of the samples were calculated from the DSC melting peaks using eq 1 and are shown in Table 4. It was inferred that the additives increased the X_c value of PLA. Melt electrospinning, on the other hand, reduced the X_c.

The relative crystallinity percentage versus time plots of the samples are shown in Figure 10. The curves had the same characteristic sigmoidal shape over time during the non-isothermal crystallization. The crystallization half-times corresponding to the 50% relative crystallinity values of the samples are listed in Table 4. The additives increased the crystallization half-times of both the filament and neat PLA fiber.

Avrami plots of the filaments and fibers are shown in Figure S1. The values of n and k are reported in Table 4. Nucleation can be classified into two types: athermal and thermal. Athermal nucleation occurs when all nuclei begin to form at approximately the same time, obtaining the same spherical (crystal) dimensions. Thermal nucleation is the nucleation through crystallization at a certain temperature, and different spherical (crystal) sizes are obtained. The Avrami constant (n) values of the filaments and fibers vary between 2.62−3.97 and

https://doi.org/10.1021/acsomega.4c09181
ACS Omega 2025, 10, 1457−1469

Table 4. Degree of Crystallinity (X_c) and Kinetic Parameters of the Filaments and Fibers Based on Nonisothermal Crystallization

	X_c [%]		n		$t_{1/2}$ [s]		$k \times 10^6$	
sample no.	filament	fiber	filament	fiber	filament	fiber	filament	fiber
1	19.63	11.54	2.62	2.75	45	35	38.11	44.15
2	27.48	20.79	3.07	2.95	44	44	5.71	9.84
3	19.81	16.02	3.97	3.09	62	72	0.03	2.04
4	24.28	17.19	3.53	3.70	60	64	0.29	0.18
5	24.58	16.67	3.19	3.95	80	117	0.17	0.02
6	25.89	16.75	2.85	3.17	62	54	9.21	1.57
7	20.43	16.24	3.71	3.52	48	81	0.06	0.88
8	30.85	20.10	3.79	3.55	49	75	0.05	0.76

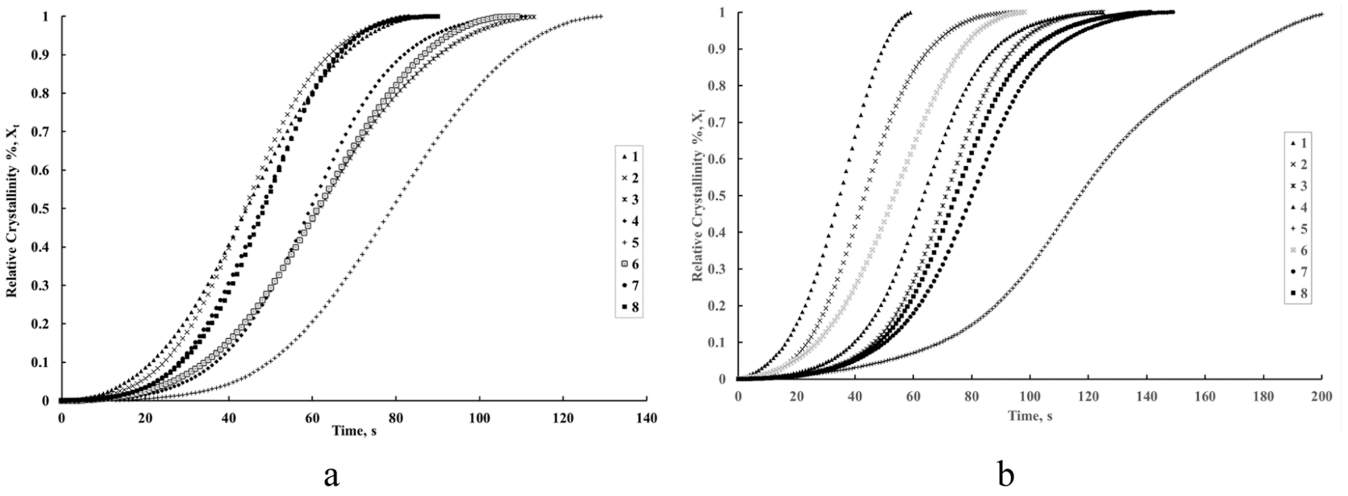

Figure 10. Relative crystallinity percentage versus time of (a) filaments and (b) fibers.

2.75−3.95, respectively. It can be said that crystallization is controlled by thermal and athermal nucleation, and the crystals have a spherical structure.[72] The crystallization rate constant k decreases with all additives, especially when the concentration of PCL is increased. The addition of 15% PCL blocked the diffusion of the PLA chains into the growing crystallites and decreased the overall crystallization rate with an increase in the nucleation rate.

The storage modulus (E'), loss modulus (E''), and loss factor ($\tan\delta$) of the filament and fiber variations with respect to temperature are shown in Figure 11. A comparison of E', E'', and $\tan\delta$ values of the filaments and fibers at 25, 60, 100, and 200 °C are listed in Table 5. The storage modulus (E') decreased with the addition of different amounts of PCL, PEG, and ZnO to PLA. This indicates that the additives decreased the hardness (increased plasticity) of PLA due to the reinforcement effect supplied by PCL, ZnO, and PEG. It has been reported that a higher storage modulus in composites indicates better adhesion between the PLA matrix and additives.[73] The E' values of the neat PLA filament and fiber at 25 °C were found to be 17.97 and 7.21 MPa, respectively. Sample 8 has a higher E' value than the other composite filaments at 25 and 60 °C, while Sample 6 has a higher E' value than the other composite filaments at 100 and 200 °C. Among the fibers, Sample 3 had the highest E' value. It can be concluded that 15% PCL, 0.1 phr ZnO, and 1 phr PEG additive provided better PCL matrix and additive adhesion in filaments and 5% PCL additive in fibers.

The loss modulus (E'') represents the viscosity of the sample. The E'' value decreased as the temperature increased. The E'' value increased with segmental mobility at ∼60 °C, which is the glass transition temperature of PLA and the melting temperature of PCL.[74]

A material with a loss factor ($\tan\delta$) < 1 exhibits less damping because its storage modulus is larger than its loss modulus. The loss factor ($\tan\delta$) of all samples was less than 1. The loss factor ($\tan\delta$) increased with increasing temperature. It has been reported that higher damping ($\tan\delta$) will lead to higher internal friction and greater mechanical losses due to the movement of molecular chains.[73]

4. CONCLUSIONS

In this study, fibers were produced by using extruded filaments and optimized melt-electrospinning process parameters. The addition of PCL, ZnO, and PEG to the neat PLA increased the fiber diameter. The minimum fiber diameter was obtained in the PLA-ZnO-PEG composite fiber (sample 2), and contact angle measurements showed that the addition of increasing PCL content (in parallel with the hydrophobic structure of PCL) and melt electrospinning improved the hydrophobic properties.

According to the TGA analysis, the addition of PCL to the PLA filament increased the degradation temperature, while the addition of ZnO and PEG decreased it. All additives reduced the degradation temperature of the spun PLA fibers. DSC analyses showed that the two polymer phases were thermodynamically immiscible, that additives increased the degree of crystallinity while decreasing the crystallization temperature, and that melt electrospinning decreased the

https://doi.org/10.1021/acsomega.4c09181
ACS Omega 2025, 10, 1457−1469

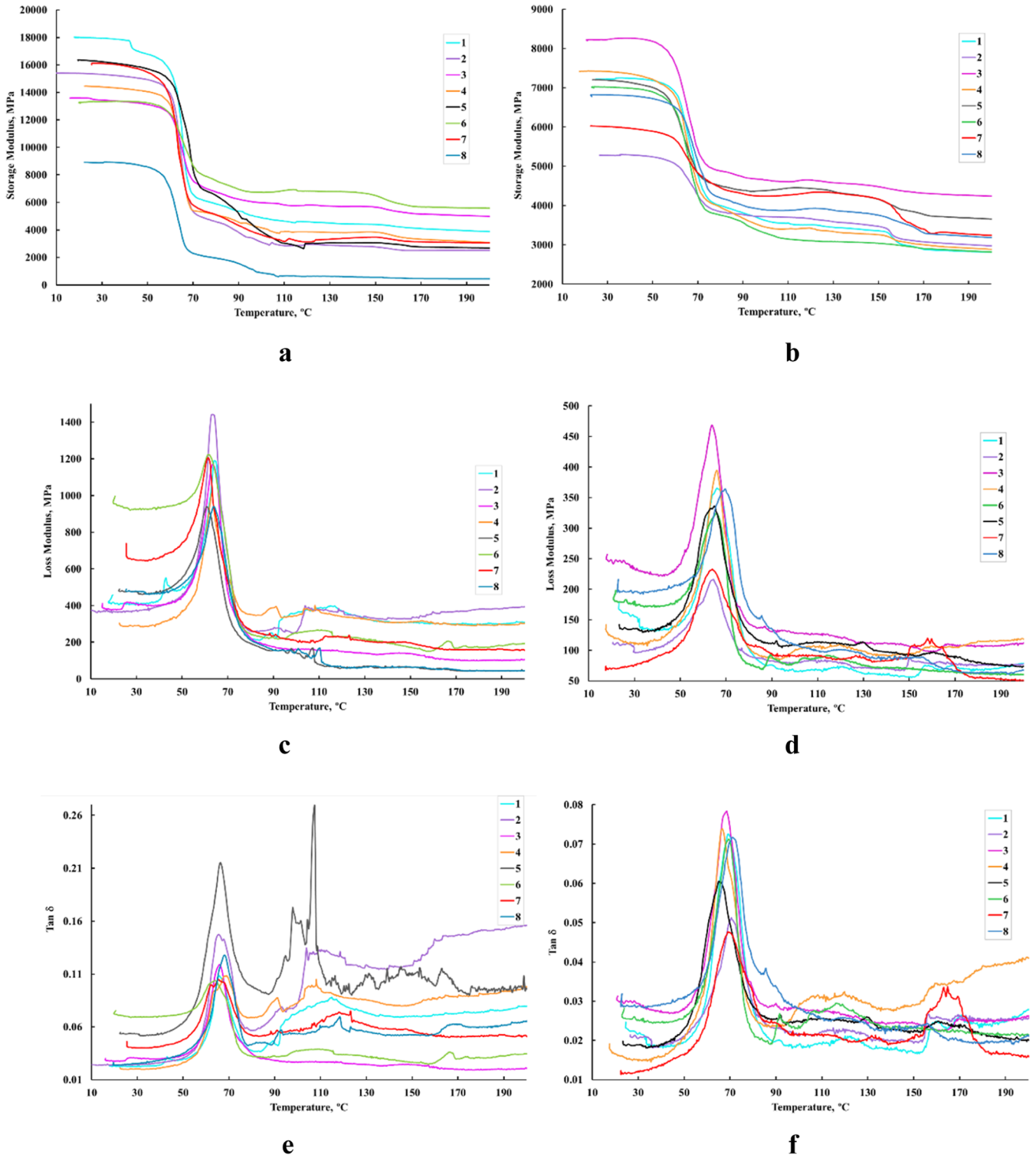

Figure 11. Storage moduli of (a) filaments and (b) fibers; loss moduli of (c) filaments and (d) fibers; and the loss factor (tan δ) of (e) filaments and (f) fibers with respect to temperature.

degree of crystallinity. Nonisothermal Avrami analysis indicated that the additives increased the crystallization half-times, crystallization took place under nucleation control, and the crystals could have a spherical structure. It was also concluded that PCL increased the nucleation rate by blocking the diffusion of PLA chains into the growing crystallites, thereby reducing the overall crystallization rate. DMA confirmed that increasing the amount of PCL increased the plasticity of the materials. The melt electrospinning method significantly improved the thermal, hydrophobic, and mechanical properties of PLA; thus, it can be programmed, aligned with the *xyz* axes, and controlled with designed shapes. The 3D structures can be created and used in packaging, drug delivery applications, wound dressings, surgical sutures, and scaffold production.

https://doi.org/10.1021/acsomega.4c09181
ACS Omega 2025, 10, 1457−1469

Table 5. Comparison of E', E'', and tan δ Values of the Filaments and Fibers at 25, 60, 100, and 200 °C

		temperature (°C)							
		25		60		100		200	
sample no.	modulus	filament	fiber	filament	fiber	filament	fiber	filament	fiber
1	E' (MPa)	17.97	7.21	15.44	6.88	4.88	3.62	3.88	2.82
	E'' (MPa)	0.41	0.18	0.81	0.22	0.36	0.07	0.31	0.08
	tan δ	0.02	0.02	0.05	0.03	0.07	0.02	0.08	0.03
2	E' (MPa)	15.35	5.28	13.89	5.07	3.09	3.72	2.52	2.97
	E'' (MPa)	0.36	0.11	0.97	0.15	0.26	0.08	0.39	0.08
	tan δ	0.02	0.02	0.07	0.03	0.08	0.02	0.16	0.03
3	E' (MPa)	13.55	8.22	12.30	7.59	5.98	4.65	4.98	4.24
	E'' (MPa)	0.39	0.25	0.80	0.33	0.16	0.13	0.10	0.11
	tan δ	0.03	0.03	0.06	0.04	0.03	0.03	0.02	0.03
4	E' (MPa)	14.44	7.43	13.03	6.79	4.16	3.45	3.09	2.89
	E'' (MPa)	0.29	0.12	0.75	0.25	0.34	0.10	0.30	0.12
	tan δ	0.02	0.02	0.06	0.04	0.08	0.03	0.10	0.04
5	E' (MPa)	8.90	7.20	6.94	6.39	0.89	4.38	0.46	3.66
	E'' (MPa)	0.48	0.13	0.92	0.31	0.14	0.11	0.04	0.07
	tan δ	0.05	0.02	0.13	0.05	0.16	0.02	0.10	0.02
6	E' (MPa)	13.32	7.03	12.43	6.43	6.72	3.29	5.57	2.81
	E'' (MPa)	0.93	0.18	1.19	0.24	0.25	0.08	0.19	0.06
	tan δ	0.07	0.03	0.10	0.04	0.04	0.02	0.03	0.02
7	E' (MPa)	16.02	6.02	13.53	5.67	3.65	4.23	3.05	3.24
	E'' (MPa)	0.74	0.07	1.15	0.15	0.21	0.09	0.16	0.05
	tan δ	0.05	0.01	0.09	0.03	0.06	0.02	0.05	0.02
8	E' (MPa)	16.32	6.82	14.80	6.51	3.90	3.89	2.69	3.19
	E'' (MPa)	0.40	0.20	0.86	0.25	0.21	0.11	0.17	0.07
	tan δ	0.02	0.03	0.06	0.04	0.05	0.03	0.07	0.02

■ ASSOCIATED CONTENT

Supporting Information

The Supporting Information is available free of charge at https://pubs.acs.org/doi/10.1021/acsomega.4c09181.

Calculated Hansen solubility parameters (Table S1), R_a and RED values (Table S2), diameters of melt-electrospun PLA fibers (Table S3), EDAX analysis of the filaments and fibers containing ZnO (Tables S4 and S5), photographs of three contact angle measurements of the filaments and fibers (Tables S6 and S7), photographs of three fiber diameter measurements (Table S8), measured diameters of the fibers (Table S9), and Avrami plot of the filaments and fibers (Figure S1). (PDF)

■ AUTHOR INFORMATION

Corresponding Author

F. Burcu Alp − *Department of Chemical Engineering, Süleyman Demirel University, Isparta 32260, Turkey;* orcid.org/0000-0002-0380-2020; Email: burcualp@sdu.edu.tr

Authors

Ferit Erdem − *Department of Chemical Engineering, Süleyman Demirel University, Isparta 32260, Turkey*

Halil Kandemir − *Department of Chemical Engineering, Süleyman Demirel University, Isparta 32260, Turkey*

Complete contact information is available at: https://pubs.acs.org/10.1021/acsomega.4c09181

Funding

This work was supported by the Scientific Research Projects Coordination Unit of Suleyman Demirel University (project code FYL-2021-8444).

Notes

The authors declare no competing financial interest.

■ REFERENCES

(1) Satti, S. M.; Shah, A. A. Polyester-Based Biodegradable Plastics: An Approach towards Sustainable Development. *Lett. Appl. Microbiol.* **2020**, *70* (6), 413−430.

(2) Basu, A.; Nazarkovsky, M.; Ghadi, R.; Khan, W.; Domb, A. J. Poly(Lactic Acid)-Based Nanocomposites. *Polym. Adv. Technol.* **2017**, *28* (8), 919−930.

(3) Kfoury, G.; Raquez, J.-M.; Hassouna, F.; Odent, J.; Toniazzo, V.; Ruch, D.; Dubois, P. Recent Advances in High Performance Poly(Lactide): From "Green" Plasticization to Super-Tough Materials via (Reactive) Compounding. *Front. Chem.* **2013**, *1*, No. 32, DOI: 10.3389/fchem.2013.00032.

(4) Auras, R. A.; Harte, B.; Selke, S.; Hernandez, R. Mechanical, Physical, and Barrier Properties of Poly(Lactide) Films. *J. Plast. Film Sheet.* **2003**, *19* (2), 123−135.

(5) Auras, R.; Harte, B.; Selke, S. Effect of Water on the Oxygen Barrier Properties of Poly(Ethylene Terephthalate) and Polylactide Films. *J. Appl. Polym. Sci.* **2004**, *92* (3), 1790−1803.

(6) Auras, R. A.; Singh, S. P.; Singh, J. J. Evaluation of Oriented Poly(Lactide) Polymers vs. Existing PET and Oriented PS for Fresh Food Service Containers. *Packag. Technol. Sci.* **2005**, *18* (4), 207−216.

(7) Lim, L. T.; Auras, R.; Rubino, M. Processing Technologies for Poly(Lactic Acid). *Prog. Polym. Sci.* **2008**, *33* (8), 820−852.

(8) Horák, Z.; Fortelný, I.; Kolařík, J.; Hlavatá, D.; Sikora, A.Polymer Blends. In *Kirk−Othmer Encyclopedia of Chemical Technology*; Wiley, 2001.

(9) Bucknall, C. B. Applications of Microscopy to the Deformation and Fracture of Rubber-Toughened Polymers. *J. Microsc.* **2001**, *201* (2), 221−229.
(10) Ahmadzadeh, Y.; Babaei, A.; Goudarzi, A. Assessment of Localization and Degradation of ZnO Nano-Particles in the PLA/PCL Biocompatible Blend through a Comprehensive Rheological Characterization. *Polym. Degrad. Stab.* **2018**, *158*, 136−147.
(11) Kelnar, I.; Kratochvíl, J.; Kaprálková, L.; Zhigunov, A.; Nevoralová, M. Graphite Nanoplatelets-Modified PLA/PCL: Effect of Blend Ratio and Nanofiller Localization on Structure and Properties. *J. Mech. Behav. Biomed. Mater.* **2017**, *71*, 271−278.
(12) Kim, C.-H.; Cho, K. Y.; Choi, E.-J.; Park, J.-K. Effect of P(LLA-Co-ECL) on the Compatibility and Crystallization Behavior of PCL/PLLA Blends. *J. Appl. Polym. Sci.* **2000**, *77* (1), 226−231.
(13) Alp, B.; Cesur, S. Isothermal Crystallization Kinetics and Mechanical Properties of Polycaprolactone Composites with Zinc Oxide, Oleic Acid, and Glycerol Monooleate. *J. Appl. Polym. Sci.* **2013**, *130* (2), 1259−1275.
(14) Shahrezaee, M.; Salehi, M.; Keshtkari, S.; Oryan, A.; Kamali, A.; Shekarchi, B. In Vitro and in Vivo Investigation of PLA/PCL Scaffold Coated with Metformin-Loaded Gelatin Nanocarriers in Regeneration of Critical-Sized Bone Defects. *Nanomedicine* **2018**, *14* (7), 2061−2073.
(15) Sartore, L.; Inverardi, N.; Pandini, S.; Bignotti, F.; Chiellini, F. PLA/PCL-Based Foams as Scaffolds for Tissue Engineering Applications. *Mater. Today Proc.* **2019**, *7*, 410−417.
(16) Hassanajili, S.; Karami-Pour, A.; Oryan, A.; Talaei-Khozani, T. Preparation and Characterization of PLA/PCL/HA Composite Scaffolds Using Indirect 3D Printing for Bone Tissue Engineering. *Mater. Sci. Eng. C* **2019**, *104*, No. 109960.
(17) Bhati, P.; Ahuja, R.; Srivastava, A.; Pankaj; Singh, S.; Vashisth, P.; Bhatnagar, N. Physicochemical Characterization and Mechanical Performance Analysis of Biaxially Oriented PLA/PCL Tubular Scaffolds for Intended Stent Application. *SN Appl. Sci.* **2020**, *2* (12), 2089.
(18) Olewnik, E.; Richert, J. Influence of the Compatibilizing Agent on Permeability and Contact Angle of Composites Based on Polylactide. *Polym. Compos* **2015**, *36* (1), 17−25.
(19) Sessini, V.; Navarro-Baena, I.; Arrieta, M. P.; Dominici, F.; López, D.; Torre, L.; Kenny, J. M.; Dubois, P.; Raquez, J. M.; Peponi, L. Effect of the Addition of Polyester-Grafted-Cellulose Nanocrystals on the Shape Memory Properties of Biodegradable PLA/PCL Nanocomposites. *Polym. Degrad. Stab.* **2018**, *152*, 126−138.
(20) Peponi, L.; Sessini, V.; Arrieta, M. P.; Navarro-Baena, I.; Sonseca, A.; Dominici, F.; Gimenez, E.; Torre, L.; Tercjak, A.; López, D.; Kenny, J. M. Thermally-Activated Shape Memory Effect on Biodegradable Nanocomposites Based on PLA/PCL Blend Reinforced with Hydroxyapatite. *Polym. Degrad. Stab.* **2018**, *151*, 36−51.
(21) Mostafa, M. H.; Elsawy, M. A.; Darwish, M. S. A.; Hussein, L. I.; Abdaleem, A. H. Microwave-Assisted Preparation of Chitosan/ZnO Nanocomposite and Its Application in Dye Removal. *Mater. Chem. Phys.* **2020**, *248*, No. 122914.
(22) Tajdari, A.; Babaei, A.; Goudarzi, A.; Partovi, R. Preparation and Study on the Optical, Mechanical, and Antibacterial Properties of Polylactic Acid/ZnO/TiO2 Shared Nanocomposites. *J. Plast. Film Sheet.* **2020**, *36* (3), 285−311.
(23) Keshavarzi, S.; Babaei, A.; Goudarzi, A.; Shakeri, A. ZnO Nanoparticles as Chain Elasticity Reducer and Structural Elasticity Enhancer: Correlating the Degradating Role and Localization of ZnO with the Morphological and Mechanical Properties of PLA/PP/ZnO Nanocomposite. *Polym. Adv. Technol.* **2019**, *30* (4), 1083−1095.
(24) Arab-Bafrani, Z.; Zabihi, E.; Jafari, S. M.; Khoshbin-Khoshnazar, A.; Mousavi, E.; Khalili, M.; Babaei, A. Enhanced Radiotherapy Efficacy of Breast Cancer Multi Cellular Tumor Spheroids through In-Situ Fabricated Chitosan-Zinc Oxide Bio-Nanocomposites as Radio-Sensitizing Agents. *Int. J. Pharm.* **2021**, *605*, No. 120828.
(25) Li, X.; Schneider, K.; Kretzschmar, B.; Stamm, M. Deformation Behavior of PP and PP/ZnO Nanocomposites As Studied by SAXS and WAXS. *Macromolecules* **2008**, *41* (12), 4371−4379.
(26) Benali, S.; Aouadi, S.; Dechief, A.-L.; Murariu, M.; Dubois, P. Key Factors for Tuning Hydrolytic Degradation of Polylactide/Zinc Oxide Nanocomposites. *Nanocomposites* **2015**, *1* (1), 51−61.
(27) Abdolmaleki, A.; Mallakpour, S.; Borandeh, S. The Use of Novel Biodegradable, Optically Active and Nanostructured Poly-(Amide-Ester-Imide) as a Polymer Matrix for Preparation of Modified ZnO Based Bionanocomposites. *Mater. Res. Bull.* **2012**, *47* (5), 1123−1129.
(28) Ahmed, J.; Arfat, Y. A.; Al-Attar, H.; Auras, R.; Ejaz, M. Rheological, Structural, Ultraviolet Protection and Oxygen Barrier Properties of Linear Low- Density Polyethylene Films Reinforced with Zinc Oxide (ZnO) Nanoparticles. *Food Packag. Shelf Life* **2017**, *13*, 20−26.
(29) Noshirvani, N.; Ghanbarzadeh, B.; Rezaei Mokarram, R.; Hashemi, M. Novel Active Packaging Based on Carboxymethyl Cellulose-Chitosan-ZnO NPs Nanocomposite for Increasing the Shelf Life of Bread. *Food Packag. Shelf Life* **2017**, *11*, 106−114.
(30) Díez-Pascual, A. M.; Díez-Vicente, A. L. Antimicrobial and Sustainable Food Packaging Based on Poly(Butylene Adipate-Co-Terephthalate) and Electrospun Chitosan Nanofibers. *RSC Adv.* **2015**, *5* (113), 93095−93107.
(31) Pantani, R.; Gorrasi, G.; Vigliotta, G.; Murariu, M.; Dubois, P. PLA-ZnO Nanocomposite Films: Water Vapor Barrier Properties and Specific End-Use Characteristics. *Eur. Polym. J.* **2013**, *49* (11), 3471−3482.
(32) Arfat, Y. A.; Ahmed, J.; Al Hazza, A.; Jacob, H.; Joseph, A. Comparative Effects of Untreated and 3-Methacryloxypropyltrimethoxysilane Treated ZnO Nanoparticle Reinforcement on Properties of Polylactide-Based Nanocomposite Films. *Int. J. Biol. Macromol.* **2017**, *101*, 1041−1050.
(33) Polat, S.; Fenercioğlu, H.; Güçlü, M. Effects of Metal Nanoparticles on the Physical and Migration Properties of Low Density Polyethylene Films. *J. Food Eng.* **2018**, *229*, 32−42.
(34) Polat, S.; Fenercioglu, H.; Unal Turhan, E.; Guclu, M. Effects of Nanoparticle Ratio on Structural, Migration Properties of Polypropylene Films and Preservation Quality of Lemon Juice. *J. Food Process. Preserv.* **2018**, *42* (4), No. e13541.
(35) Díez-Pascual, A. M.; Díez-Vicente, A. L. ZnO-Reinforced Poly(3-Hydroxybutyrate-Co-3-Hydroxyvalerate) Bionanocomposites with Antimicrobial Function for Food Packaging. *ACS Appl. Mater. Interfaces* **2014**, *6* (12), 9822−9834.
(36) Liu, H.; Zhang, J. Research Progress in Toughening Modification of Poly(Lactic Acid). *J. Polym. Sci., Part B: Polym. Phys.* **2011**, *49* (15), 1051−1083.
(37) Kulinski, Z.; Piorkowska, E. Crystallization, Structure and Properties of Plasticized Poly(l-Lactide). *Polymer* **2005**, *46* (23), 10290−10300.
(38) Hu, Y.; Hu, Y. S.; Topolkaraev, V.; Hiltner, A.; Baer, E. Crystallization and Phase Separation in Blends of High Stereoregular Poly(Lactide) with Poly(Ethylene Glycol). *Polymer* **2003**, *44* (19), 5681−5689.
(39) Sheth, M.; Ananda Kumar, R.; Dav, V.; Gross, R. A.; McCarthy, S. P. Biodegradable Polymer Blends of Poly(Lactic Acid) and Poly(Ethylene Glycol). *J. Appl. Polym. Sci.* **1997**, *66*, 1495−1505.
(40) Kumar, T. S. M.; Senthil Kumar, K.; Rajini, N.; Siengchin, S.; Ayrilmis, N.; Varada Rajulu, A. A Comprehensive Review of Electrospun Nanofibers: Food and Packaging Perspective. *Composites, Part B* **2019**, *175*, No. 107074.
(41) Tang, Y.; Zhou, Y.; Lan, X.; Huang, D.; Luo, T.; Ji, J.; Mafang, Z.; Miao, X.; Wang, H.; Wang, W. Electrospun Gelatin Nanofibers Encapsulated with Peppermint and Chamomile Essential Oils as Potential Edible Packaging. *J. Agric. Food Chem.* **2019**, *67* (8), 2227−2234.
(42) Sun, B.; Long, Y. Z.; Zhang, H. D.; Li, M. M.; Duvail, J. L.; Jiang, X. Y.; Yin, H. L. Advances in Three-Dimensional Nanofibrous

https://doi.org/10.1021/acsomega.4c09181
ACS Omega 2025, 10, 1457−1469

Macrostructures via Electrospinning. *Prog. Polym. Sci.* **2014**, *39* (5), 862−890.
(43) Babar, A. A.; Iqbal, N.; Wang, X.; Yu, J.; Ding, B.Introduction and Historical Overview. In *Electrospinning: Nanofabrication and Applications*; Elsevier, 2019; pp 3−20.
(44) Xue, J.; Wu, T.; Dai, Y.; Xia, Y. Electrospinning and Electrospun Nanofibers: Methods, Materials, and Applications. *Chem. Rev.* **2019**, *119* (8), 5298−5415.
(45) Antunes, M. D.; da Silva Dannenberg, G.; Fiorentini, Â. M.; Pinto, V. Z.; Lim, L. T.; da Rosa Zavareze, E.; Dias, A. R. G. Antimicrobial Electrospun Ultrafine Fibers from Zein Containing Eucalyptus Essential Oil/Cyclodextrin Inclusion Complex. *Int. J. Biol. Macromol.* **2017**, *104*, 874−882.
(46) Yu, W.; Guo, J.; Liu, Y.; Xue, X.; Wang, X.; Wei, L.; Mao, L.; Zhang, Z.; Zhuo, Y.; Li, S.; Ma, J.; Xu, D. Fabrication of Novel Electrospun Zein/Polyethylene Oxide Film Incorporating Nisin for Antimicrobial Packaging. *LWT* **2023**, *185*, No. 115176.
(47) Moreno, M. A.; Orqueda, M. E.; Gómez-Mascaraque, L. G.; Isla, M. I.; López-Rubio, A. Crosslinked Electrospun Zein-Based Food Packaging Coatings Containing Bioactive Chilto Fruit Extracts. *Food Hydrocolloids* **2019**, *95*, 496−505.
(48) Azeredo, H. M. C.; Barud, H.; Farinas, C. S.; Vasconcellos, V. M.; Claro, A. M. Bacterial Cellulose as a Raw Material for Food and Food Packaging Applications. *Front. Sustainable Food Syst.* **2019**, *3*, No. 7, DOI: 10.3389/fsufs.2019.00007.
(49) Kara, H. H.; Xiao, F.; Sarker, M.; Jin, T. Z.; Sousa, A. M. M.; Liu, C.-K.; Tomasula, P. M.; Liu, L. Antibacterial Poly(Lactic Acid) (PLA) Films Grafted with Electrospun PLA/Allyl Isothiocyanate Fibers for Food Packaging. *J. Appl. Polym. Sci.* **2016**, *133* (2), No. 42475, DOI: 10.1002/app.42475.
(50) Lan, W.; Liang, X.; Lan, W.; Ahmed, S.; Liu, Y.; Qin, W. Electrospun Polyvinyl Alcohol/d-Limonene Fibers Prepared by Ultrasonic Processing for Antibacterial Active Packaging Material. *Molecules* **2019**, *24* (4), No. 767.
(51) Salević, A.; Prieto, C.; Cabedo, L.; Nedović, V.; Lagaron, J. M. Physicochemical, Antioxidant and Antimicrobial Properties of Electrospun Poly(ε-Caprolactone) Films Containing a Solid Dispersion of Sage (Salvia Officinalis L.) Extract. *Nanomaterials* **2019**, *9* (2), No. 270.
(52) Liu, Y.; Li, K.; Mohideen, M.; Ramakrishna, S.Development of Melt Electrospinning: The Past, Present, and Future. In *Melt Electrospinning*; Wiley, 2019; pp 1−5.
(53) Rivera, M. L.; Hudson, S. E.et al. In *Desktop Electrospinning: A Single Extruder 3D Printer for Producing Rigid Plastic and Electrospun Textiles*, Proceedings of the 2019 CHI Conference on Human Factors in Computing Systems, 2019.
(54) Shahverdi, M.; Seifi, S.; Akbari, A.; Mohammadi, K.; Shamloo, A.; Movahhedy, M. R. Melt Electrowriting of PLA, PCL, and Composite PLA/PCL Scaffolds for Tissue Engineering Application. *Sci. Rep.* **2022**, *12* (1), No. 19935.
(55) Li, X.; Zhang, S.; Li, J.; Hu, X.; Zhang, J.; Wei, Q.; Zhang, C.; Zhang, D.; Liu, Y. Bio-Degradable Fibrous Membranes for Oil/Water Separation by Melt Electrospinning. *J. Appl. Polym. Sci.* **2024**, *141* (39), No. 56018.
(56) Lian, H.; Meng, Z. Melt Electrospinning vs. Solution Electrospinning: A Comparative Study of Drug-Loaded Poly (ε-Caprolactone) Fibres. *Mater. Sci. Eng. C* **2017**, *74*, 117−123.
(57) Sarwar, Z.; Krugly, E.; Danilovas, P. P.; Ciuzas, D.; Kauneliene, V.; Martuzevicius, D. Fabrication and Characterization of PEBA Fibers by Melt and Solution Electrospinning. *J. Mater. Res. Technol.* **2019**, *8* (6), 6074−6085.
(58) Hansen, C. M. *Hansen Solubility Parameters: A User's Handbook*, 2nd ed.; CRC Press, 2007.
(59) Li, C.; Dou, Q. Non-Isothermal Crystallization Kinetics and Spherulitic Morphology of Nucleated Poly(Lactic Acid): Effect of Dilithium Hexahydrophthalate as a Novel Nucleating Agent. *Thermochim. Acta* **2014**, *594*, 31−38.
(60) Janeschitz-Kriegl, H. *Crystallization Modalities in Polymer Melt Processing*; Springer, 2018.
(61) Valenti, S.; del Valle, L.; Yousefzade, O.; Macovez, R.; Franco, L.; Puiggalí, J. Chloramphenicol Loaded Polylactide Melt Electrospun Scaffolds for Biomedical Applications. *Int. J. Pharm.* **2021**, *606*, No. 120897.
(62) Yu, S.-X.; Zheng, J.; Yan, X.; Wang, X.-X.; Nie, G.-D.; Tan, Y.-Q.; Zhang, J.; Sui, K.-Y.; Long, Y.-Z. Morphology Control of PLA Microfibers and Spheres via Melt Electrospinning. *Mater. Res. Express* **2018**, *5* (4), No. 045019.
(63) Nazari, T.; Garmabi, H. The Effects of Processing Parameters on the Morphology of PLA/PEG Melt Electrospun Fibers. *Polym. Int.* **2018**, *67* (2), 178−188.
(64) Chieng, B. W.; Ibrahim, N. A.; Yunus, W. M. Z. W.; Hussein, M. Z. Poly(Lactic Acid)/Poly(Ethylene Glycol) Polymer Nanocomposites: Effects of Graphene Nanoplatelets. *Polymers* **2014**, *6* (1), 93−104.
(65) Choksi, N.; Desai, H. Synthesis of Biodegradable Polylactic Acid Polymer by Using Lactic Acid Monomer. *Int. J. Appl. Chem.* **2017**, *13* (2), 377−384.
(66) Kemala, T.; Budianto, E.; Soegiyono, B. Preparation and Characterization of Microspheres Based on Blend of Poly(Lactic Acid) and Poly(E-Caprolactone) with Poly(Vinyl Alcohol) as Emulsifier. *Arab. J. Chem.* **2012**, *5* (1), 103−108.
(67) Elzein, T.; Nasser-Eddine, M.; Delaite, C.; Bistac, S.; Dumas, P. FTIR Study of Polycaprolactone Chain Organization at Interfaces. *J. Colloid Interface Sci.* **2004**, *273* (2), 381−387.
(68) Sahu, M.; Reddy, V. R. M.; Kim, B.; Patro, B.; Park, C.; Kim, W. K.; Sharma, P. Fabrication of Cu2ZnSnS4 Light Absorber Using a Cost-Effective Mechanochemical Method for Photovoltaic Applications. *Materials* **2022**, *15* (5), No. 1708.
(69) Al-Hajry, A.; Umar, A.; Hahn, Y.; Kim, D.-H. Growth, Properties and Dye-Sensitized Solar Cells−Applications of ZnO Nanorods Grown by Low-Temperature Solution Process. *Superlattices Microstruct.* **2009**, *45*, 529−534.
(70) Dwivedi, C.; Pandey, I.; Pandey, H.; Ramteke, P. W.; Pandey, A. C.; Mishra, S. B.; Patil, S.Electrospun Nanofibrous Scaffold as a Potential Carrier of Antimicrobial Therapeutics for Diabetic Wound Healing and Tissue Regeneration. In *Nano- and Microscale Drug Delivery Systems: Design and Fabrication*; Elsevier B.V., 2017; pp 147−164.
(71) Sharma, D.; Satapathy, B. K. Optimization and Physical Performance Evaluation of Electrospun Nanofibrous Mats of PLA, PCL and Their Blends. *J. Ind. Text.* **2022**, *51* (4_suppl), 6640S−6665S.
(72) Dhanvijay, P. U.; Shertukde, V. V. Review: Crystallization of Biodegradable Polymers. *Polym. Plast. Technol. Eng.* **2011**, *50* (13), 1289−1304.
(73) Huda, M. S.; Drzal, L. T.; Mohanty, A. K.; Misra, M. Effect of Fiber Surface-Treatments on the Properties of Laminated Biocomposites from Poly(Lactic Acid) (PLA) and Kenaf Fibers. *Compos. Sci. Technol.* **2008**, *68* (2), 424−432.
(74) Sharma, D.; Satapathy, B. K. Performance Evaluation of Electrospun Nanofibrous Mats of Polylactic Acid (PLA)/Poly (ε-Caprolactone) (PCL) Blends. *Mater. Today Proc.* **2019**, *19*, 188−195.

https://doi.org/10.1021/acsomega.4c09181
ACS Omega 2025, 10, 1457−1469